ACS OMEGA

Open Access

http://pubs.acs.org/journal/acsodf

Article

Microwave-Assisted Biosynthesis of Quercetin-Stabilized Gold Nanoparticles with Enhanced Antibacterial and Catalytic Properties

Yodchai Tangjaideborisut, Paramasivam Shanmugam,* Alvin Lim Teik Zheng, Pariya Na Nakorn,* and Supakorn Boonyuen*

Cite This: *ACS Omega* 2025, 10, 17327−17336

Read Online

ACCESS | Metrics & More | Article Recommendations

ABSTRACT: In the past few years, substantial progress has been made in the field of microwave-assisted biosynthesis of gold nanoparticles (AuNPs) using quercetin (QT) as a natural reducing and stabilizing agent. This study explores the rapid and eco-friendly synthesis of AuNPs facilitated by microwave irradiation, offering a time-efficient alternative to conventional methods. The AuNPs were thoroughly characterized to confirm their morphology, size, crystalline structure, and surface plasmon resonance (SPR). The synthesized AuNPs were confirmed by visual color change from yellow to violet and characteristic SPR peak at 519 nm. Furthermore, XRD studies clearly confirmed the crystalline nature of the face-centered cubic structure of AuNPs. Moreover, TEM images reveal that the AuNPs were found to be more or less spherical and have a slightly variable morphology with an average diameter of 14 nm. The antibacterial properties of QT and AuNPs were evaluated against two different bacterial strains via *Staphylococcus aureus* and *Escherichia coli*, demonstrating significant activity, particularly due to the stabilizing effect of QT. Additionally, the catalytic efficiency of the AuNPs was evaluated by their ability to reduce 4-nitrophenol to 4-aminophenol, a model reaction for the catalytic activity. The results were promising, with the rate constant of QT-AuNPs determined to be 0.1016 s^{-1}. This work highlights the dual functionality of QT-mediated AuNPs in enhancing both antimicrobial and catalytic properties, contributing to their potential applications in the biomedical and environmental fields. This study highlights the dual role of QT-mediated AuNPs in enhancing antimicrobial and catalytic properties, paving the way for innovative applications in both the biomedical and environmental fields. The uniqueness lies in leveraging the natural properties of QT to simultaneously improve biological activity and catalytic efficiency, offering a sustainable and multifunctional QT-AuNP solution.

1. INTRODUCTION

The development of nanomaterials, particularly metal nanoparticles, has attracted significant attention due to their unique physicochemical properties and wide-ranging applications in fields such as catalysis, medicine, and environmental science. Noble metal nanoparticles—including silver, gold, palladium, platinum, and ruthenium—have been especially noted for their potential in medical and industrial applications.[1,2] Among these, AuNPs stand out for their stability, biocompatibility, and catalytic properties, making them ideal candidates for various industrial and biomedical uses.[3,4] However, a key challenge lies in synthesizing AuNPs through eco-friendly, efficient, and selective methods that avoid toxic chemicals.[5,6] In this context, the use of natural biomolecules as stabilizing agents presents a promising green chemistry approach.[7,8] Nguyen et al. reported the biosynthesis of AuNPs using *Ganoderma lucidum* extract via a microwave-assisted method, which produced smaller AuNPs in a shorter reaction time.[9] Green synthesis of AuNPs demonstrated excellent catalytic activity in reducing 4-nitrophenol to 4-aminophenol, along with high stability, maintaining performance through four catalytic cycles.[3,9]

The biomolecule of quercetin (QT) is of greater interest for the green synthesis of metal nanoparticles.[10] The QT-containing flavonoid has antioxidant properties, which can act as both a reducing and stabilizing agent for AuNP synthesis.[11] Various methods have been employed to synthesize AuNPs, including chemical reduction, microwave-assisted synthesis, biological methods, seed-mediated growth, polyol reduction, laser ablation, sol−gel techniques, electrochemical synthesis, ultrasonic synthesis, and chemical vapor deposition.[12−14] Among these, the microwave-assisted synthesis using QT has proven to be a powerful method for

Received: November 13, 2024
Revised: February 19, 2025
Accepted: February 24, 2025
Published: April 25, 2025

producing AuNPs with uniform particle size distribution, enhanced purity, and shorter reaction times.[15] The rapid heating and uniform energy distribution provided by microwave irradiation significantly improve the synthesis process compared to conventional techniques.[16,17] In the case of AuNP synthesis, microwave irradiation accelerates the reduction of gold ions, facilitating the formation of stable nanoparticles when natural stabilizers, such as QT, are used. This combination of microwave irradiation and QT stabilization presents a green and efficient route for AuNP synthesis with potential applications in catalytic and biomedical fields. Parthiban et al. reported the green synthesis of AuNPs stabilized by QT, a biomolecule derived from mangrove plants. The synthesized AuNPs exhibited remarkable fluorescence properties and demonstrated significant anticancer activity against A549 and HeLa cell lines.[11] The catalytic activity of AuNPs, particularly in hydrogenation reactions, has been extensively studied due to their ability to facilitate electron transfer and lower activation energies.[18]

Hydrogenation plays a crucial role in organic chemistry by converting unsaturated compounds into saturated ones.[19] QT-AuNPs are hypothesized to offer enhanced catalytic performance and antimicrobial activity due to the synergistic effects of the nanoparticles' surface properties and QT's functional groups.[20−22] Shen et al. reported the hydrogenation of 4-NP using AuNPs with a cell-free extract of *Aspergillus* sp.[18] Particularly, the AuNPs have high resistance of pathogens, thus strongly exhibiting antimicrobial activity by disrupting microbial cell membranes and interfering with cellular functions.[23,24] QT, with its inherent antioxidant and antimicrobial properties, may further enhance the biological activity of AuNPs, offering a dual-function system for both catalytic and antimicrobial uses.

Therefore, this study aims to investigate the microwave-assisted green synthesis of QT-stabilized AuNPs and evaluate their catalytic efficiency in hydrogenation reactions, as well as their antimicrobial potential against various pathogens. In addition, the optical and morphological properties, crystal structure, and particle size distribution of AuNPs were examined. This present study investigates microwave-assisted QT-stabilized AuNPs to explore the dual functionality of the QT-AuNP system, offering a promising approach for the development of sustainable materials with applications in green chemistry and biomedical fields.

2. DISCUSSION

2.1. UV−Visible Spectrum Analysis of QT-AuNPs. The UV−visible absorption spectra of the QT-AuNPs measured at different time intervals (10, 30, 60, and 100 min) exhibit characteristic features indicative of the formation of gold nanoparticles and growth over time (Figure 1). The pure form QT spectrum shows no significant absorption in the visible region, thus indicating that pure QT does not contain any nanoparticles. After the addition of $HAuCl_4$, a well-defined surface plasmon resonance (SPR) band begins to emerge around 520−525 nm, which is typical for the formation of spherical AuNPs. At 10 min, a weak SPR band is observed at approximately 530 nm, suggesting the early stages of nanoparticle nucleation.[25−27] As the reaction time progresses, the intensity of the SPR band increases, reaching a maximum around 60 min, which correlates with the growth of the AuNPs. This increase in the intensity corresponds to the progressive accumulation of free electrons, leading to a more

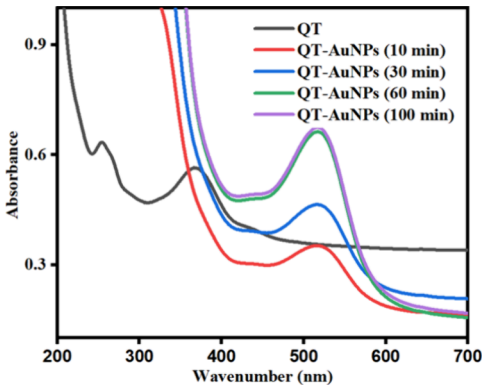

Figure 1. UV−visible spectra of the AuNPs.

pronounced plasmonic effect. The SPR peak position remains constant at 100 min, thus indicating that Au^{3+} ions may have been completely converted into Au^0.[28,29] Furthermore, in the lower wavelength region (300−400 nm), the absorbance increases, which may also indicate contributions from the QT-AuNP complex, possibly related to interactions between QT (QT) and the AuNP surface. These results demonstrate that both the size and the concentration of AuNPs increase with time, as evidenced by the evolving UV−visible spectra.

2.2. FTIR Study of QT and QT-AuNPs. The FTIR spectra of QT and QT-functionalized gold nanoparticles (QT-AuNPs) are shown in Figure 2. FTIR spectroscopy was used to identify

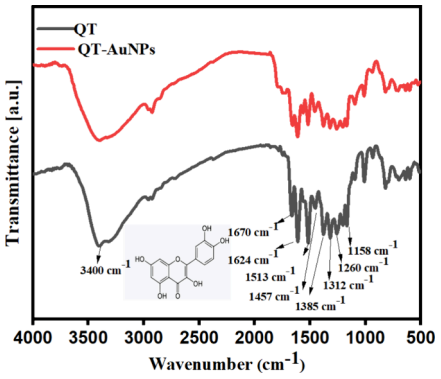

Figure 2. FTIR spectra of QT and QT-AuNPs.

the functional groups in pure QT and to examine any changes in these groups after the stabilization of AuNPs. The broad absorption peak observed around 3400 cm^{-1} corresponds to O−H stretching vibrations, indicative of hydroxyl groups present in the QT structure. This broad peak is characteristic of phenolic hydroxyl groups, which are known for forming strong hydrogen bonds. Additionally, a strong peak at 1670 cm^{-1} is attributed to C═O stretching vibrations of the carbonyl group in the QT molecule, which is a key feature of the flavonoid backbone. The intensity of this peak suggests a well-defined presence of conjugated carbonyl functionalities.

The absorption band around 1513−1624 cm^{-1} corresponds to C═C stretching vibrations of the aromatic rings, confirming the presence of QT's phenyl groups. Furthermore, the bands observed in the range of 1260−1385 cm^{-1} are assigned to C−O stretching, providing evidence of phenolic ethers and hydroxyl groups in QT. In the FTIR spectrum of QT-AuNPs, significant peak shifts are observed. The broad O−H and C═O stretching bands are slightly reduced in intensity, indicating

https://doi.org/10.1021/acsomega.4c10323
ACS Omega 2025, 10, 17327−17336

interactions between the hydroxyl groups of QT and the surface of the gold nanoparticles.[30,31] This suggests that the hydroxyl groups play a role in stabilizing and binding QT to the gold nanoparticle surface.[8,32] Additionally, the C═O stretching peak at 1650 cm^{-1} shifts to a lower wavenumber in the QT-AuNP spectrum, implying coordination between the C═O group and the AuNPs. This interaction decreases the vibrational energy of the C═O bond, confirming the successful functionalization of AuNPs with QT. These spectral findings are consistent with the successful functionalization of AuNPs, where QT acts as both a reducing and capping agent, stabilizing the AuNPs through its functional groups. This is crucial for the development of AuNP systems with potential biomedical applications.

2.3. XRD Spectrum Analysis of AuNPs. The X-ray diffraction (XRD) spectrum primarily helps to analyze the crystalline structure and phase purity of the as-prepared materials and the corresponding spectrum shown in Figure 3.

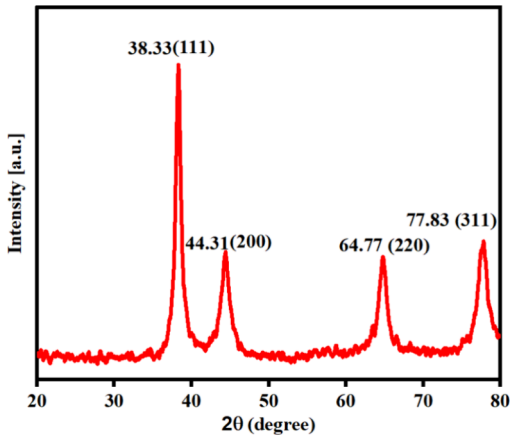

Figure 3. XRD spectra of the AuNPs.

The XRD pattern of the synthesized AuNPs reveals distinct diffraction peaks at 38.33°, 44.31°, 64.77°, and 77.83°, corresponding to the (111), (200), (220), and (311) crystallographic planes of face-centered cubic (FCC) gold, respectively (JCPDS file no. 04-0784).[33] The intense peak at 38.33° associated with the (111) plane indicates a predominant growth orientation, which is typical for AuNPs, suggesting that the (111) plane is the most stable and energetically favorable. The presence of sharp, well-defined peaks confirms the crystalline nature of the AuNPs. The broadening of the peaks can be attributed to the nanoscale dimensions of the AuNPs, as smaller particles tend to exhibit broader diffraction peaks due to the Scherrer effect. For the determination of fwhm values, we used Origin software. In this case, we utilized the peak with a maximum intensity at 38.33° and calculated the fwhm value as 0.95065. Based on this fwhm value, the crystallite size was found to be 9.24 nm. Additionally, the absence of extra peaks indicates the high purity of the AuNPs, with no significant contamination from other crystalline phases.

2.4. Morphological Study. The surface morphology and elemental composition of the synthesized QT-AuNPs were characterized by using FESEM and EDAX analyses, as shown in Figure 4a,b. The corresponding elemental composition values are listed in Figure 4b. Figure 4a reveals spherical white spots with uniform sizes ranging from approximately 16.5 to 26.8 nm, confirming the successful formation of AuNPs. Additionally, the black layer observed in the image corresponds to the organic moiety of QT, which stabilizes the AuNPs.[34] The small and uniform particle sizes of the QT-AuNPs enhance the surface-to-volume ratio, which is crucial for catalytic applications, such as the reduction of 4-NP to 4-AP and antibacterial activities. Figure 4b shows the elemental composition of the QT-AuNPs, as determined by EDAX analysis. The results indicate that the prepared QT-AuNPs contain significant amounts of carbon (C), oxygen (O), and gold (Au). Carbon and oxygen are the predominant elements, with weight percentages of 56.63 and 26.66%, respectively, likely originating from the base material or the organic components of QT. Gold is detected with a weight percentage of 16.36%, confirming the successful incorporation of Au nanoparticles, which are expected to enhance photocatalytic and electronic properties. Additionally, trace amounts of silicon (0.27%) and chlorine (0.08%) are observed, which may arise from residual precursors or minor contamination during the synthesis process. This analysis confirms the successful synthesis of QT-AuNPs with the desired morphology and elemental composition, supporting their potential applicability in catalytic and antibacterial applications.

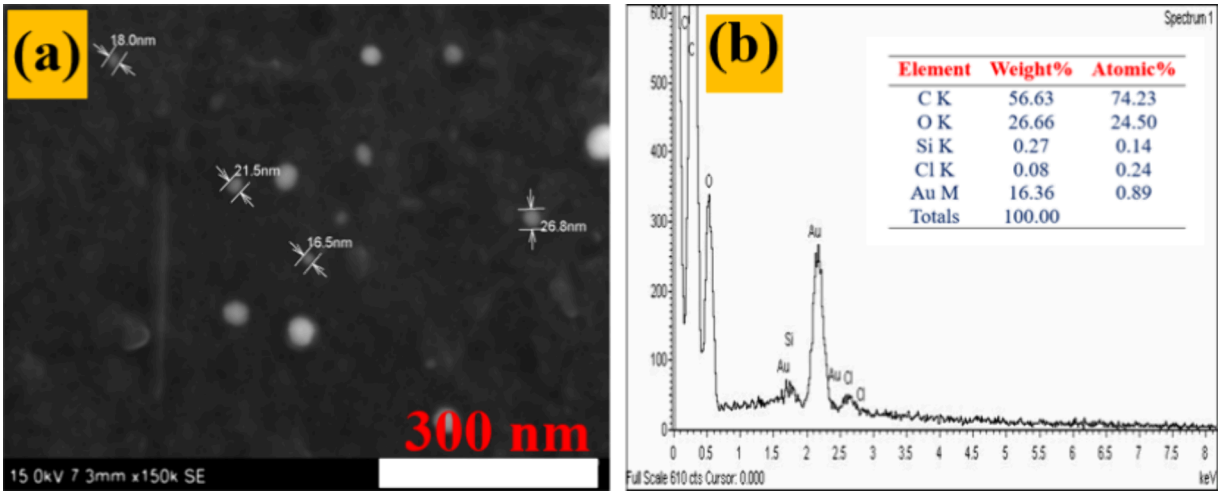

Figure 4. (a) FESEM and (b) EDAX images of the QT-AuNPs.

https://doi.org/10.1021/acsomega.4c10323
ACS Omega 2025, 10, 17327−17336

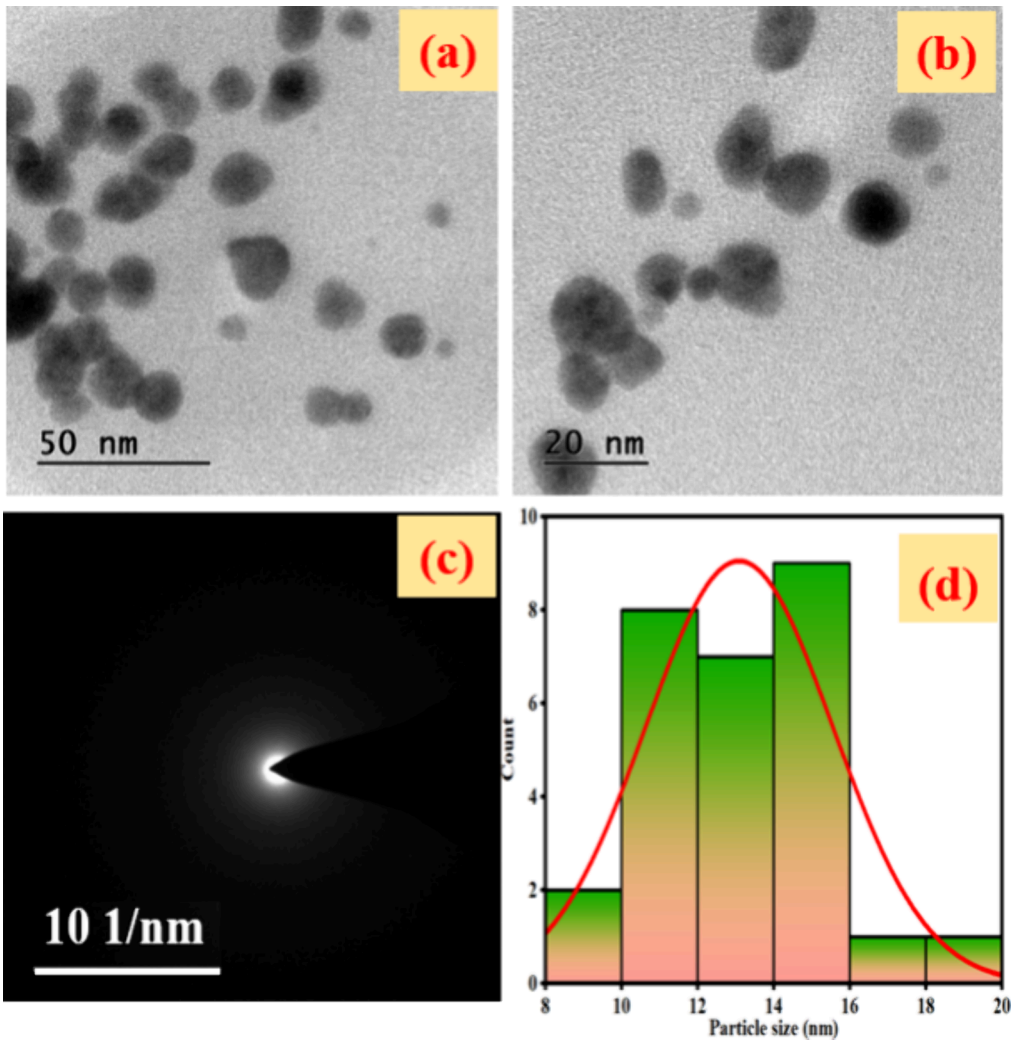

Figure 5. TEM images of the AuNPs: (a) Low magnification, (b) high magnification, (c) SAED pattern, and (d) particle size distribution curve.

The TEM analysis provided detailed information about the as-prepared AuNPs at very high resolution, typically at the atomic or molecular level. The TEM images of the synthesized AuNPs are shown in Figure 5a,b. Figure 5a reveals the morphology and distribution of the AuNPs, which are predominantly spherical with slight size variations. The particles are well-dispersed with minimal agglomeration, indicating good stability. Furthermore, the observed particles range in size from approximately 10−20 nm, with more detail visible in the higher magnification image in Figure 5b. Figure 5c shows surface-induced diffraction of the AuNPs, displaying a distinct ring pattern that confirms their crystalline nature. This ring pattern can be attributed to the face-centered cubic (FCC) structure of the AuNPs, further affirming the successful synthesis of crystalline nanoparticles.[35] The particle size distribution, as illustrated in the histogram in Figure 5d, indicates that the synthesized AuNPs predominantly fall within the size range of 10−16 nm, with an average particle size of approximately 14 nm. The relatively narrow distribution highlights the uniformity of the AuNP synthesis process. QT plays an important role in stabilizing the particle size, which is crucial for enhancing their catalytic and antimicrobial properties. Overall, the TEM results demonstrate that the prepared AuNPs are spherical and crystalline and exhibit a relatively narrow size distribution, contributing to improved catalytic activity and high toxicity against bacteria and fungi.

2.5. Catalytic Activity of AuNPs. The catalytic efficiency of the AuNPs was examined through the reduction of 4-NP by $NaBH_4$ in the presence of AuNPs as catalysts. In this case, aqueous $NaBH_4$ is considered relatively eco-friendly due to the low toxicity of borates and its thermodynamically favorable reaction (E^0 for 4-NP/4-AP = −0.76 V and H_3BO_3/BH_4^- = −1.33 V). Figure 6 shows the UV−vis spectra of catalytic reduction of 4-NP; in label (a), the absorbance peaks are observed at 326 nm.[3,36] After the addition of $NaBH_4$, the 326 nm peak shifted to 401 nm, which confirmed the formation 4-nitrophenolate ions (4-NP^-). This peak diminishes over time as the reaction progresses, indicating the reduction of 4-NP to 4-aminophenol (4-AP).[37] The reduction is evidenced by the simultaneous decrease in the intensity of the 400 nm peak and the appearance of a new peak near 300 nm, labeled as (b), which corresponds to the formation of 4-AP. The spectra clearly demonstrate the dependent reduction, with distinct absorption changes at intervals of 0−24 min. At 0 min, the absorption peak at 400 nm is strong, indicating the presence of 4-nitrophenolate. When the reaction was initiated, the peak intensity of 401 nm decreased, while the intensity of the peak at 300 nm increased, signifying the production of 4-AP. The peak at 401 nm almost completely disappears within 24 min,

https://doi.org/10.1021/acsomega.4c10323
ACS Omega 2025, 10, 17327−17336

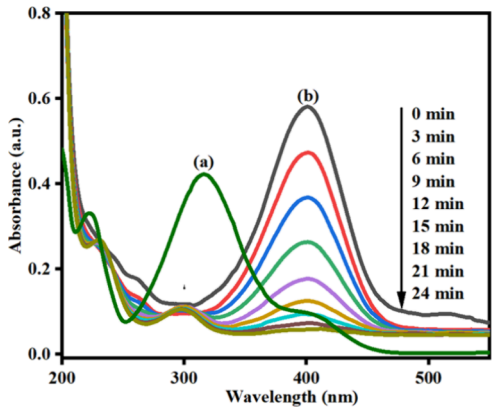

Figure 6. UV−visible spectra of the reduction of 4-NP using AuNPs.

thus confirming the near completion of the reduction reaction. The AuNPs serve as an efficient catalyst for this reaction, facilitating electron transfer from $NaBH_4$ to 4-NP, resulting in the reduction to 4-AP. The steady decrease in the absorption at 400 nm and the corresponding increase in absorption at 300 nm demonstrate the catalytic efficiency and stability of the AuNPs.[38] The time-dependent UV−vis spectra confirm the effective role of AuNPs in accelerating the reduction process of 4-NP, making this system highly suitable for environmental remediation applications involving nitroaromatic pollutants.

Based on the UV−visible spectrum, the kinetic plots for the reduction of 4-nitrophenol (4-NP) in the presence of AuNPs are illustrated in Figure 7a,b. Figure 7a shows the time-

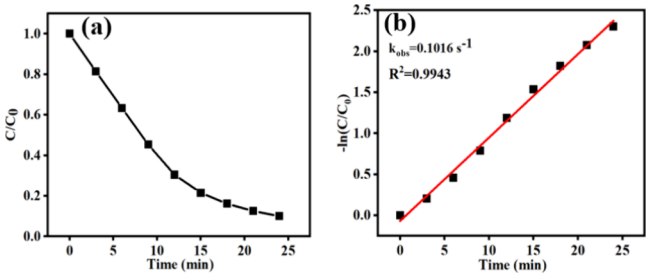

Figure 7. (a) Time-dependent plot for reduction of 4-NP and (b) kinetic plots for the reduction of 4-NP in the presence of AuNPs.

dependent decrease in the normalized concentration of 4-NP (C/C_0) vs time. The concentration of 4-NP decreases steadily, indicating that the catalytic reduction follows a consistent reaction pathway. At the initial stage, the sharp initial decline in concentration, followed by a slower reduction toward the end, reveals that the AuNPs facilitate a rapid reaction at the initial stage, which then slows as the substrate concentration decreases. Figure 7b represents the pseudo-first-order kinetic model for the reduction process. Figure 7b plotted by $-\ln(C/C_0)$ Vs time shows a strong linear correlation ((R^2 = 0.9943), indicating that the reaction follows pseudo-first-order kinetics with respect to the concentration of 4-NP, when an excess amount of $NaBH_4$ is present. The observed rate constant for the reduction reaction is calculated as 0.1016 s^{-1}, demonstrating the catalytic efficiency of AuNPs in the reduction process. The high R^2 value confirms the reliability of the kinetic model, and the relatively large rate constant suggests that the AuNPs provide an effective surface for electron transfer, facilitating the reduction of 4-NP to 4-AP. The results reinforce the role of AuNPs as efficient nanocatalysts, making them suitable for applications in catalytic transformations, especially in environmental remediation processes. Furthermore, Table 1 presents

Table 1. Comparison of Catalytic Reduction of 4-NP to 4-AP by Various AuNPs

catalysts	reducing agents	rate constant	time	particle size	ref
Au NPs	$NaBH_4$	0.360 min^{-1}	9	24.1	42
Au/CD_100_3	$NaBH_4$	0.660 min^{-1}	9	5.3	42
Au(0)@TpPa-1	$NaBH_4$	5.35 × 10^{-3} s^{-1}	13		43
Au/GO NPs	$NaBH_4$	0.368 min^{-1}	10	5	44
Au NPs	$NaBH_4$	0.36 min^{-1}	14	24.1	45
QT-AuNPs	$NaBH_4$	0.1016 s^{-1}	24	14	this work

the rate constant values for the catalytic reduction of 4-NP to 4-AP using various types of AuNP catalysts reported in previous studies. These differences may be attributed to variations in the structure, size, reaction time, and composition of the nanoparticles. It is evident that the reduction of 4-NP is significantly influenced by the structure, size, and composition of the nanoparticles.

Figure 8 illustrates the proposed mechanism for the catalytic reduction of 4-NP to 4-AP. In this process, $NaBH_4$ serves as

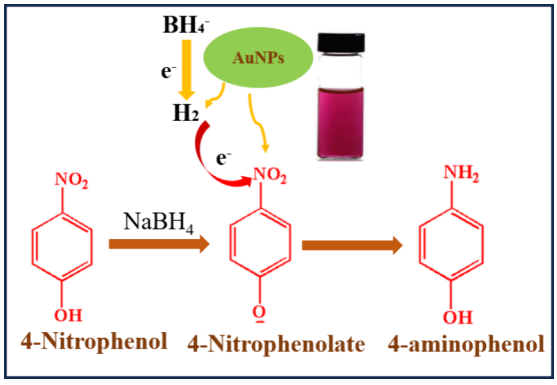

Figure 8. Possible mechanism of the reduction of 4-NP to 4-AP.

both an electron donor and a hydrogen source, while the QT-AuNPs function as electron transfer mediators. The QT-AuNPs facilitate the transfer of electrons from the borohydride ion (BH_4^-) to 4-NA, enabling the reduction reaction.[39,40] Hydrogen species from BH_4^- and 4-NA are rapidly adsorbed onto the surface of QT-AuNPs, and the diffusion of these adsorbed species on the nanoparticle surface results in the desorption of the product 4-AP. Additionally, the QT-AuNPs play a crucial role as an electron relay to sustain the reduction process. The small, spherical QT-AuNPs possess a high surface area-to-volume ratio, providing a greater number of active catalytic sites compared to larger nanoparticles. Conversely, larger QT-AuNPs experience increased steric interactions between the adsorbed reactant species, which can hinder adsorption and subsequently reduce the reaction rate.[41] This highlights the significance of the nanoparticle size in optimizing catalytic activity.

2.6. Antibacterial Activity. The antibacterial activity of QT against *S. aureus* and *E. coli* was examined through a well-diffusion method. The results are depicted in Figure 9a,b, and the corresponding zone inhibition values are given in Table 2.

https://doi.org/10.1021/acsomega.4c10323
ACS Omega 2025, 10, 17327−17336

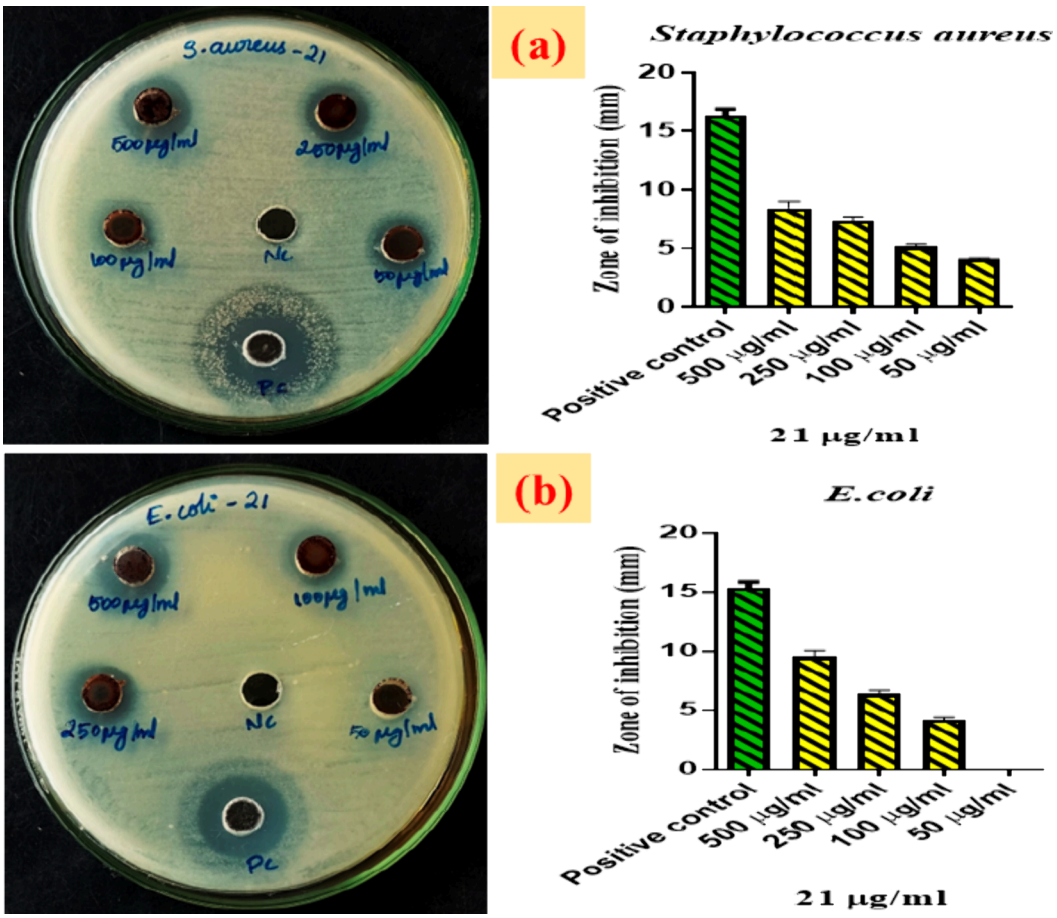

Figure 9. Antibacterial activity of QT against (a) *S. aureus* and (b) *E. coli*.

Table 2. Antibacterial Activity of QT and QT-AuNPs

	zone of Inhibition (mm)				
	S. aureus				
sample name	500 μg/mL	250 μg/mL	100 μg/mL	50 μg/mL	positive control
QT	8.4 ± 0.56	7.3 ± 042	5.15 ± 0.21	4.1 ± 0.14	16.35 ± 0.49
QT-AuNPs	15.75 ± 1.06	12.35 ± 0.49	6.2 ± 0.28	5.15 ± 0.21	18.4 ± 0.56
	E. coli				
QT	9.45 ± 0.6	6.3 ± 0.42	4.15 ± 0.21	0	15.35 ± 0.49
QT-AuNPs	14.5 ± 0.707	11.35 ± 0.49	5.3 ± 0.42	4.2 ± 0.28	16.75 ± 1.06

The zone of inhibition was measured for varying concentrations of QT (500, 250, 100, and 50 μg/mL), with a positive control to compare efficacy.[46,47] Figure 9a shows the antibacterial activity of *S. aureus*, and the obtained results reveal that QT exhibited a significant inhibitory effect, with the largest zone of inhibition observed at the highest concentration of 500 μg/mL, indicating strong antibacterial activity. The zone of inhibition gradually decreased as the concentration reduced, with the lowest inhibition observed at 50 μg/mL. This dose-dependent effect suggests that higher concentrations of QT are required for effective bacterial inhibition. Furthermore, Figure 9b displays the antibacterial effect of *E. coli*, and the obtained results show a similar trend, where QT inhibits bacterial growth more effectively at higher concentrations. However, the overall zone of inhibition was smaller compared to that of *S. aureus*, indicating that QT is less effective against *E. coli*. At 500 μg/mL, the inhibition was significant; however, as the concentration dropped, the antibacterial effect diminished. Finally, QT showed promising antibacterial properties, especially against *S. aureus*, but was less effective against *E. coli*. The results suggest that the Gram-positive bacterium (*S. aureus*) is more susceptible to QT than the Gram-negative bacterium (*E. coli*), which may be due to structural differences in their cell walls. These findings support QT's potential use as a natural antimicrobial agent; however, further studies are required to enhance its effectiveness, especially against Gram-negative bacteria.

Furthermore, the antibacterial activity of the QT-AuNPs was assessed against the same *S. aureus* and *E. coli* using a well-diffusion assay, as illustrated in Figure 10a,b, and the corresponding zone inhibition values are given in Table 2. The inhibition zones for different concentrations of AuNPs (500, 250, 100, and 50 μg/mL) were measured with positive controls used for comparison. Figure 10a shows the *S. aureus* well plate, and the results demonstrate that AuNPs possess significant antibacterial activity. The highest concentration of

https://doi.org/10.1021/acsomega.4c10323
ACS Omega 2025, 10, 17327−17336

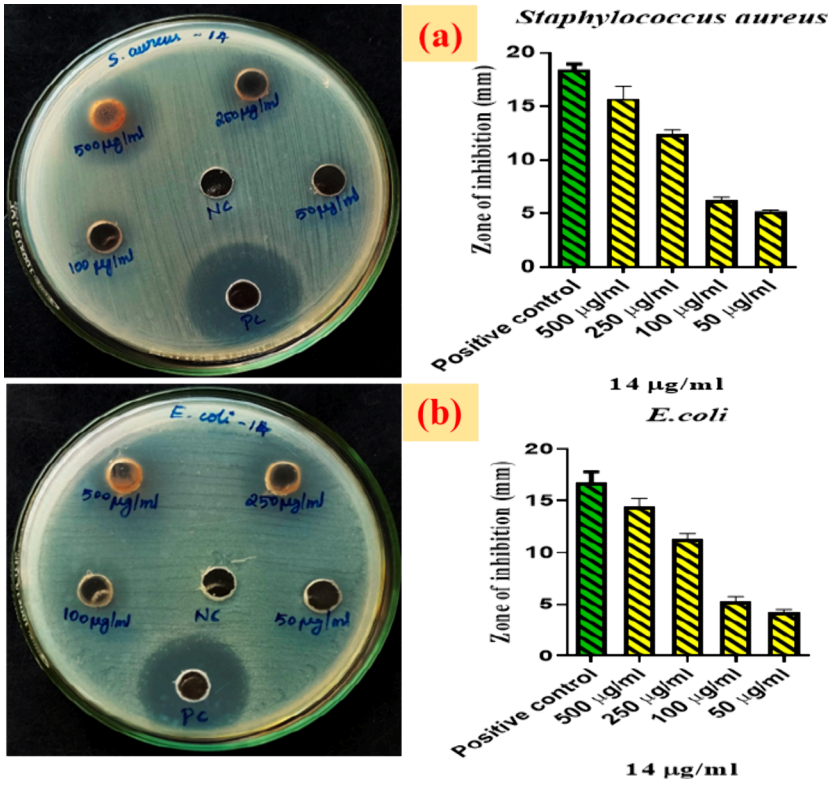

Figure 10. Antibacterial activity of QT-AuNPs against (a) *S. aureus* and (b) *E. coli*.

500 μg/mL produced the largest zone of inhibition, which steadily decreased with lower concentrations. The 100 and 50 μg/mL concentrations showed reduced but measurable inhibition, indicating a concentration-dependent antibacterial effect. The strong inhibitory action of AuNPs against *S. aureus* suggests their potential as an effective antimicrobial agent against Gram-positive bacteria. Furthermore, similar trends appeared in *E. coli* bacteria, as shown in Figure 10b. The highest concentration (500 μg/mL) yielded a substantial zone of inhibition, indicating good antibacterial efficacy. However, the zones of inhibition were smaller compared to those seen for *S. aureus*, particularly at lower concentrations, such as 50 μg/mL. This finding suggests that while AuNPs are effective against *E. coli*, the Gram-negative bacterium is less susceptible to their antibacterial effects compared to the Gram-positive *S. aureus*. The comparative analysis between the two bacteria indicates that AuNPs exhibit stronger antibacterial activity against *S. aureus* than *E. coli*. This may be attributed to the differences in cell wall structure between Gram-positive and Gram-negative bacteria, where the thicker peptidoglycan layer in Gram-positive bacteria could allow more interaction with AuNPs. Furthermore, AuNPs present a promising antimicrobial agent, particularly against Gram-positive bacteria like *S. aureus*, though their efficacy against Gram-negative bacteria like *E. coli* could benefit from further optimization or increased concentrations. On comparing the antibacterial activity of QT and QT-AuNPs, QT-AuNPs show superior antibacterial activity compared with QT, possibly due to enhanced penetration and bioavailability, particle size, surface area, synergistic effect of AuNPs, intrinsic antibacterial properties of AuNPs, solubility, etc. Table 3 displays the diameter of the inhibition zone values compared with different AuNPs. The obtained results reveal that QT-AuNPs show better antibacterial performance than QT. Vijayaraghavan et al. reported that the metal nanoparticles can easily penetrate the bacterial cell wall, leading to increased cell permeability and subsequent cell death.[48]

Table 3. Diameter of Inhibition Zone of *E. coli* and *S. aureus* Bacteria Using Different AuNPs

	diameter of inhibition zone (mm)		
sample	*E. coli* (mm)	*S. aureus* (mm)	ref
Oi-AuNPs	5.46	-	49
AuNPs	28	25	50
AuNPs	6	2	51
AuNPs	25	12.5	52
QT-AuNPs	14.5	15.75	this study

3. CONCLUSIONS

In summary, this study demonstrates the successful microwave-assisted biosynthesis of QT-stabilized gold nanoparticles (QT-AuNPs), providing a rapid, eco-friendly, and efficient method for nanoparticle production. The synthesized AuNPs exhibited favorable characteristics, including a face-centered cubic crystalline structure, a spherical morphology with an average size of 14 nm, and a distinct SPR peak at 519 nm. The QT-mediated stabilization enhanced both the antimicrobial and catalytic properties of the AuNPs, showing significant antibacterial activity against *S. aureus* and *E. coli*, as well as effective catalytic performance in the reduction of 4-NP. The QT-AuNPs show outstanding catalytic properties, with the rate constant value found to be 0.1016 s^{-1}. These findings highlight the potential applications of QT-AuNPs in the biomedical and environmental fields, emphasizing their dual functionality in antimicrobial and catalytic processes.

https://doi.org/10.1021/acsomega.4c10323
ACS Omega 2025, 10, 17327−17336

4. EXPERIMENTAL SECTION

4.1. Materials. QT was purchased from Sigma-Aldrich Pvt. Ltd., USA. Chloroauric acid ($HAuCl_4 \cdot 3H_2O$) was purchased from Loba Chemie Pvt. Ltd., Mumbai, India. Sodium borohydride ($NaBH_4$), 4-NP, ammonium hydroxide (NH_4OH, 25%), acetone, agar−agar solution, and ethanol (99%) were obtained from Sigma-Aldrich, USA. All chemicals were used as received without further purification.

4.2. Synthesis of AuNPs. The AuNPs were synthesized by QT using the microwave irradiation process.[49] In a typical process, 10 mL of 1 mM chloroauric acid was added to 10 mL of QT dissolved in ethanol. For the preparation process with the assistance of microwave irradiation, the reaction mixture was placed in a microwave oven to react for 10 min at 400 W. The colloidal AuNPs were precipitated using 95% ethanol (v/v), followed by centrifugation (4000 rpm, 20 min). The pellets obtained were then dried in an oven at 100 °C for 12 h and stored for studying both the physicochemical characteristics and the catalytic activity (Scheme 1).

Scheme 1. Schematic Representation of the Synthesis of AuNPs Using QT

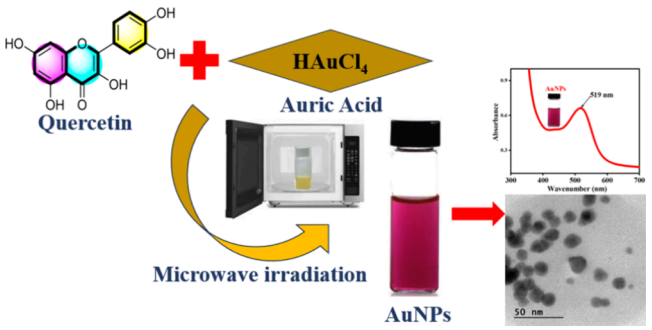

4.3. Catalytic Activity of AuNPs. The catalytic efficiency of AuNPs in the reduction of 4-NP was evaluated in an aqueous solution at room temperature.[49,53] In a typical procedure, 250 μL of 1 mM 4-NP, 250 μL of 0.1 M sodium borohydride ($NaBH_4$), and 2 mL of deionized water were placed in a quartz cuvette. Following this, 1 mg of AuNPs was introduced into the cuvette, and the reaction was monitored by using a UV−vis spectrophotometer. The reduction process was tracked by recording the UV−vis spectra at regular time intervals within a wavelength range of 200−500 nm to observe changes in the absorption profile of the reaction mixture.

4.4. Antibacterial Activity. The antibacterial properties of QT and QT-AuNPs were evaluated against *S. aureus* and *E. coli* using Nutrient Agar medium. Initially, 20 mL of nutrient agar was poured into Petri plates and seeded with a 24 h culture. Wells containing *S. aureus* 902 and *E. coli* 443 were treated with different concentrations of QT and AuNPs (500, 250, 100, and 50 μg/mL). The plates were incubated at 37 °C for 24 h. Antibacterial activity was assessed by measuring the diameter of the inhibition zones, which were formed around the wells.[54] Gentamicin (10 μL) was used as a positive control. The data were analyzed using GraphPad Prism 6.0 software (USA).

4.5. Characterization. The green synthesis of AuNPs and the optical properties of these samples were examined using a UV−vis V-630 spectrophotometer. The crystal structure and phase purity of the prepared AuNPs were examined through XRD (D8-Bruker, Germany) equipped with CuKα radiation (λ = 1.5406 Å). The particle size, distribution, and surface morphology of the synthesized AuNPs were observed using a transmission electron microscope (JEOL-1010, Japan) integrated with a scanning electron microscope (JEOL JSM-6510, Japan). Moreover, the elemental and atomic weight composition of the samples were examined by EDX. Furthermore, to identify the functional groups of multiple biomolecules in these samples, FTIR analysis was then performed using an R-Prestige-21 Shimadzu FTIR spectrophotometer using the KBr pellet method.

■ ASSOCIATED CONTENT

Data Availability Statement

Data will be made available on request.

■ AUTHOR INFORMATION

Corresponding Authors

Paramasivam Shanmugam − *Department of Chemistry, Faculty of Science and Technology, Thammasat University, Pathumthani 12120, Thailand;* orcid.org/0000-0002-9535-8771; Email: shanmugachem@gmail.com

Pariya Na Nakorn − *Department of Biotechnology, Faculty of Science and Technology, Thammasat University, Pathumthani 12120, Thailand*; Email: pariya_n@sci.tu.ac.th

Supakorn Boonyuen − *Department of Chemistry, Faculty of Science and Technology, Thammasat University, Pathumthani 12120, Thailand*; Email: chemistrytu@gmail.com

Authors

Yodchai Tangjaideborisut − *Department of Biotechnology, Faculty of Science and Technology, Thammasat University, Pathumthani 12120, Thailand*

Alvin Lim Teik Zheng − *Department of Science and Technology, Faculty of Humanities, Management and Science, Universiti Putra Malaysia, Bintulu 97008 Sarawak, Malaysia*

Complete contact information is available at: https://pubs.acs.org/10.1021/acsomega.4c10323

Author Contributions

Y.T.: Conceptualization, methodology, formal analysis, investigation, data curation, and writing—review and editing. P.S.: Writing—original draft, writing—review and editing, A.L.T.Z.: Formal analysis, data curation, and writing—review and editing, S.B.: Supervision, data curation, and writing—review and editing. P.N.N.: Supervision, Investigation, resources, and writing—review and editing.

Notes

The authors declare no competing financial interest.

■ ACKNOWLEDGMENTS

This work was supported by the Thailand Science Research and Innovation Fundamental Fund (TU-FF32/2568). This research has received funding support from the NSRF via the Program Management Unit for Human Resources & Institutional Development, Research and Innovation (No. B05F640151). Furthermore, the author greatly acknowledges FOODMATRIX GLOBAL CO., LTD, for continuous financial and characterization supports.

REFERENCES

(1) El-Tantawy, A. I.; Elsaeed, S. M.; Neiber, R. R.; Eisa, W. H.; Aleem, A. A. H. A.; El-Hamalawy, A. A.; Maize, M. S. Silver Nanoparticles-Based Thioureidophosphonate Composites: Synthesis Approach and Their Exploitation in 4-Nitrophenol Reduction. *Surfaces and Interfaces* **2023**, *40*, No. 103006.

(2) Noël, S.; Bricout, H.; Addad, A.; Sonnendecker, C.; Zimmermann, W.; Monflier, E.; Léger, B. Catalytic Reduction of 4-Nitrophenol with Gold Nanoparticles Stabilized by Large-Ring Cyclodextrins. *New J. Chem.* **2020**, *44* (48), 21007−21011.

(3) Kästner, C.; Thünemann, A. F. Catalytic Reduction of 4-Nitrophenol Using Silver Nanoparticles with Adjustable Activity. *Langmuir* **2016**, *32* (29), 7383−7391.

(4) Prabhakar, U. P. S.; Shanmugam, P.; Boonyuen, S.; Chandrasekar, L. P.; Pothu, R.; Boddula, R.; Radwan, A. B.; Al-Qahtani, N. Non-Covalent Functionalization of Surfactant-Assisted Graphene Oxide with Silver Nanocomposites for Highly Efficient Photocatalysis and Anti-Biofilm Applications. *Materials Science for Energy Technologies* **2024**, *7*, 205−215.

(5) Khan, Md. A. R.; Al Mamun, M. S.; Habib, Md. A.; Islam, A. B. M. N.; Mahiuddin, Md.; Karim, K. M. R.; Naime, J.; Saha, P.; Dey, S. K.; Ara, M. H. A Review on Gold Nanoparticles: Biological Synthesis, Characterizations, and Analytical Applications. *Resultsin Chemistry* **2022**, *4*, No. 100478.

(6) Salesa, B.; Ferrús-Manzano, P.; Tuñón-Molina, A.; Cano-Vicent, A.; Assis, M.; Andrés, J.; Serrano-Aroca, Á. Study of Biological Properties of Gold Nanoparticles: Low Toxicity, No Proliferative Activity, No Ability to Induce Cell Gene Expression and No Antiviral Activity. *Chemico-Biological Interactions* **2023**, *382*, No. 110646.

(7) Shanmugam, P.; Boonyuen, S.; Tangjaideborisu, Y.; Na Nakorn, P.; Tantayanon, S.; Pothu, R.; Boddula, R. Anthocyanin Rich-Berry Extracts Coated Magnetic Fe_3O_4 Bionanocomposites and Their Antibacterial Activity. *Inorg. Chem. Commun.* **2023**, *156*, No. 111291.

(8) Ranjana, R.; Parushuram, N.; Harisha, K. S.; Narayana, B.; Sangappa, Y. Photo-Driven Synthesis of Anisotropic Gold Nanoparticles Using Silk Fibroin—Cell Viability Activities in Lymphocyte and Jurkat Cancer Cells. *BioNanoSci.* **2020**, *10* (4), 864−875.

(9) Nguyen, V. P.; Le Trung, H.; Nguyen, T. H.; Hoang, D.; Tran, T. H. Advancement of Microwave-Assisted Biosynthesis for Preparing Au Nanoparticles Using Ganoderma Lucidum Extract and Evaluation of Their Catalytic Reduction of 4-Nitrophenol. *ACS Omega* **2021**, *6* (47), 32198−32207.

(10) Sareethammanuwat, M.; Boonyuen, S.; Arpornmaeklong, P. Effects of Beta-Tricalcium Phosphate Nanoparticles on the Properties of a Thermosensitive Chitosan/Collagen Hydrogel and Controlled Release of Quercetin. *J. Biomed. Mater. Res., Part A* **2021**, *109* (7), 1147−1159.

(11) Parthiban, A.; Sachithanandam, V.; Sarangapany, S.; Misra, R.; Muthukrishnan, P.; Jeyakumar, T. C.; Purvaja, R.; Ramesh, R. Green Synthesis of Gold Nanoparticles Using Quercetin Biomolecule from Mangrove Plant, *Ceriops Tagal*: Assessment of Antiproliferative Properties, Cellular Uptake and DFT Studies. *J. Mol. Struct.* **2023**, *1272*, No. 134167.

(12) Kobayashi, Y.; Correa-Duarte, M. A.; Liz-Marzán, L. M. Sol−Gel Processing of Silica-Coated Gold Nanoparticles. *Langmuir* **2001**, *17* (20), 6375−6379.

(13) Ohara, Y.; Akazawa, K.; Shibata, K.; Hirota, T.; Kodama, Y.; Amemiya, T.; Wang, J.; Yamaguchi, T. Seed-Mediated Gold Nanoparticle Synthesis via Photochemical Reaction of Benzoquinone. *Colloids Surf., A* **2020**, *586*, No. 124209.

(14) Gao, L.; Mei, S.; Ma, H.; Chen, X. Ultrasound-Assisted Green Synthesis of Gold Nanoparticles Using Citrus Peel Extract and Their Enhanced Anti-Inflammatory Activity. *Ultrasonics Sonochemistry* **2022**, *83*, No. 105940.

(15) Arshi, N.; Ahmed, F.; Kumar, S.; Anwar, M. S.; Lu, J.; Koo, B. H.; Lee, C. G. Microwave Assisted Synthesis of Gold Nanoparticles and Their Antibacterial Activity against *Escherichia coli* (*E. coli*). *Curr. Appl. Phys.* **2011**, *11*, S360−S363.

(16) Perveen, K.; Husain, F. M.; Qais, F. A.; Khan, A.; Razak, S.; Afsar, T.; Alam, P.; Almajwal, A. M.; Abulmeaty, M. M. A. Microwave-Assisted Rapid Green Synthesis of Gold Nanoparticles Using Seed Extract of Trachyspermum Ammi: ROS Mediated Biofilm Inhibition and Anticancer Activity. *Biomolecules* **2021**, *11* (2), 197.

(17) Huang, M.; Xiong, E.; Wang, Y.; Hu, M.; Yue, H.; Tian, T.; Zhu, D.; Liu, H.; Zhou, X. Fast Microwave Heating-Based One-Step Synthesis of DNA and RNA Modified Gold Nanoparticles. *Nat. Commun.* **2022**, *13* (1), 968.

(18) Shen, W.; Qu, Y.; Pei, X.; Li, S.; You, S.; Wang, J.; Zhang, Z.; Zhou, J. Catalytic Reduction of 4-Nitrophenol Using Gold Nanoparticles Biosynthesized by Cell-Free Extracts of *Aspergillus* Sp. WL-Au. *Journal of Hazardous Materials* **2017**, *321*, 299−306.

(19) Shanmugaraj, K.; Bustamante, T. M.; Torres, C. C.; Campos, C. H. Gold Nanoparticles Supported on Mesostructured Oxides for the Enhanced Catalytic Reduction of 4-Nitrophenol in Water. *Catal. Today* **2022**, *388*−*389*, 383−393.

(20) Das, D. Kr.; Chakraborty, A.; Bhattacharjee, S.; Dey, S. Biosynthesis of Stabilised Gold Nanoparticle Using an Aglycone Flavonoid, Quercetin. *Journal of Experimental Nanoscience* **2013**, *8* (4), 649−655.

(21) Liu, Y.; Zhou, H.; Yin, T.; Gong, Y.; Yuan, G.; Chen, L.; Liu, J. Quercetin-Modified Gold-Palladium Nanoparticles as a Potential Autophagy Inducer for the Treatment of Alzheimer's Disease. *J. Colloid Interface Sci.* **2019**, *552*, 388−400.

(22) Milanezi, F. G.; Meireles, L. M.; de Christo Scherer, M. M.; de Oliveira, J. P.; da Silva, A. R.; de Araujo, M. L.; Endringer, D. C.; Fronza, M.; Guimarães, M. C. C.; Scherer, R. Antioxidant, Antimicrobial and Cytotoxic Activities of Gold Nanoparticles Capped with Quercetin. *Saudi Pharmaceutical Journal* **2019**, *27* (7), 968−974.

(23) Sathiyaraj, S.; Suriyakala, G.; Dhanesh Gandhi, A.; Babujanarthanam, R.; Almaary, K. S.; Chen, T.-W.; Kaviyarasu, K. Biosynthesis, Characterization, and Antibacterial Activity of Gold Nanoparticles. *Journal of Infection and Public Health* **2021**, *14* (12), 1842−1847.

(24) Fu, L.-H.; Yang, J.; Zhu, J.-F.; Ma, M.-G. Synthesis of Gold Nanoparticles and Their Applications in Drug Delivery. In *Metal Nanoparticles in Pharma*, Rai, Ph. D., Mahendra, Shegokar, Ph. D., Ranjita, Eds.; Springer International Publishing: Cham, 2017; pp 155−191.

(25) Cui, X.; Liu, M.; Li, B. Homogeneous Fluorescence-Based Immunoassay via Inner Filter Effect of Gold Nanoparticles on Fluorescence of CdTe Quantum Dots. *Analyst* **2012**, *137* (14), 3293−3299.

(26) Amendola, V.; Meneghetti, M. Size Evaluation of Gold Nanoparticles by UV−vis Spectroscopy. *J. Phys. Chem. C* **2009**, *113* (11), 4277−4285.

(27) Sakthisabarimoorthi, A.; Martin Britto Dhas, S. A.; Jose, M. Preparation of Composite Ag@Au Core−Shell Nanoparticles and Their Linear and Nonlinear Optical Properties. *J. Mater. Sci: Mater. Electron* **2019**, *30* (2), 1677−1685.

(28) López-Muñoz, G. A.; Pescador-Rojas, J. A.; Ortega-Lopez, J.; Salazar, J. S.; Balderas-López, J. A. Thermal Diffusivity Measurement of Spherical Gold Nanofluids of Different Sizes/Concentrations. *Nanoscale Res. Lett.* **2012**, *7* (1), 423.

(29) Zeng, S.; Yong, K.-T.; Roy, I.; Dinh, X.-Q.; Yu, X.; Luan, F. A Review on Functionalized Gold Nanoparticles for Biosensing Applications. *Plasmonics* **2011**, *6* (3), 491−506.

(30) Murugan, E.; Shanmugam, P. Efficient Functionalization of Poly(Styrene) Beads Immobilized Metal Nanoparticle Catalysts for the Reduction of Crystal Violet. *Bull. Mater. Sci.* **2015**, *38* (3), 629−637.

(31) Khan, S.; Runguo, W.; Tahir, K.; Jichuan, Z.; Zhang, L. Catalytic Reduction of 4-Nitrophenol and Photo Inhibition of *Pseudomonas Aeruginosa* Using Gold Nanoparticles as Photocatalyst. *Journal of Photochemistry and Photobiology B: Biology* **2017**, *170*, 181−187.

(32) Harisha, K. S.; Parushuram, N.; Asha, S.; Suma, S. B.; Narayana, B.; Sangappa, Y. Eco-Synthesis of Gold Nanoparticles by Sericin

https://doi.org/10.1021/acsomega.4c10323
ACS Omega 2025, 10, 17327−17336

Derived from Bombyx Mori Silk and Catalytic Study on Degradation of Methylene Blue. *Particulate Science and Technology* **2021**, *39* (2), 131−140.
(33) Sneha, K.; Esterle, A.; Sharma, N.; Sahi, S. Yucca-Derived Synthesis of Gold Nanomaterial and Their Catalytic Potential. *Nanoscale Res. Lett.* **2014**, *9*, 627.
(34) Mioc, M.; Pavel, I. Z.; Ghiulai, R.; Coricovac, D. E.; Farcaş, C.; Mihali, C.-V.; Oprean, C.; Serafim, V.; Popovici, R. A.; Dehelean, C. A.; Shtilman, M. I.; Tsatsakis, A. M.; Şoica, C. The Cytotoxic Effects of Betulin-Conjugated Gold Nanoparticles as Stable Formulations in Normal and Melanoma Cells. *Front. Pharmacol.* **2018**, *9*, 429.
(35) Tadi, A. T.; Farhadiannezhad, M.; Nezamtaheri, M. S.; Goliaei, B.; Nowrouzi, A. Biosynthesis and Characterization of Gold Nanoparticles from Citrullus Colocynthis (L.) Schrad Pulp Ethanolic Extract: Their Cytotoxic, Genotoxic, Apoptotic, and Antioxidant Activities. *Heliyon* **2024**, *10* (16), No. e35825.
(36) Bijalwan, K.; Kainthola, A.; Sharma, H.; Dwivedi, C. Catalytic Reduction of 4-Nitrophenol Using Gold-Silver Alloy Nanoparticles Coated on Alkali Activated Sand. *Materials Today: Proceedings* **2020**, *28*, 1097−1100.
(37) Das, T. K.; Das, N. Ch. Advances on Catalytic Reduction of 4-Nitrophenol by Nanostructured Materials as Benchmark Reaction. *Int. Nano Lett.* **2022**, *12* (3), 223−242.
(38) Suneetha, M.; Min Ji, S.; Kim, E.; Uthappa, U. T.; Soo Han, S. High Efficient Dip Catalyst for Nitrophenol Reduction Using Bacterial Cellulose Impregnated Self-Crosslinked Glycol Chitosan via Formation of Gold Nanoparticles. *Mater. Lett.* **2024**, *370*, No. 136781.
(39) Karanam, L.; Janardhana, C.; R, M.; Rao, A. M.; Gangula, A.; Podila, R. Catalytic Reduction of 4-Nitrophenol Using Biogenic Gold and Silver Nanoparticles Derived from Breynia Rhamnoides. *Langmuir* **2011**, *27* (24), 15268−15274.
(40) Edison, T. N. J. I.; Baral, E. R.; Lee, Y. R.; Kim, S. H. Biogenic Synthesis of Silver Nanoparticles Using Cnidium Officinale Extract and Their Catalytic Reduction of 4-Nitroaniline. *J. Clust Sci.* **2016**, *27* (1), 285−298.
(41) Reddy, V.; Torati, R. S.; Oh, S.; Kim, C. Biosynthesis of Gold Nanoparticles Assisted by Sapindus Mukorossi Gaertn. Fruit Pericarp and Their Catalytic Application for the Reduction of p-Nitroaniline. *Ind. Eng. Chem. Res.* **2013**, *52* (2), 556−564.
(42) Rodríguez Molina, H.; Santos Muñoz, J. L.; Domínguez Leal, M. I.; Reina, T. R.; Ivanova, S.; Centeno Gallego, M. Á.; Odriozola, J. A. Carbon Supported Gold Nanoparticles for the Catalytic Reduction of 4-Nitrophenol. *Front. Chem.* **2019**, *7*, 548.
(43) Zeng, J.; Zhang, Q.; Chen, J.; Xia, Y. A Comparison Study of the Catalytic Properties of Au-Based Nanocages, Nanoboxes, and Nanoparticles. *Nano Lett.* **2010**, *10* (1), 30−35.
(44) Wu, T.; Zhang, L.; Gao, J.; Liu, Y.; Gao, C.; Yan, J. Fabrication of Graphene Oxide Decorated with Au−Ag Alloy Nanoparticles and Its Superior Catalytic Performance for the Reduction of 4-Nitrophenol. *J. Mater. Chem. A* **2013**, *1* (25), 7384−7390.
(45) Berahim, N.; Basirun, W. J.; Leo, B. F.; Johan, M. R. Synthesis of Bimetallic Gold-Silver (Au-Ag) Nanoparticles for the Catalytic Reduction of 4-Nitrophenol to 4-Aminophenol. *Catalysts* **2018**, *8* (10), 412.
(46) da Costa, T. S.; da Silva, M. R.; Barbosa, J. C. J.; Neves, U. D. S. D.; de Jesus, M. B.; Tasic, L. Biogenic Silver Nanoparticles' Antibacterial Activity and Cytotoxicity on Human Hepatocarcinoma Cells (Huh-7). *RSC Adv.* **2024**, *14* (4), 2192−2204.
(47) Maniah, K.; Olyan Al-Otibi, F.; Mohamed, S.; Said, B. A.; Ragab AbdelGawwad, M.; Taha Yassin, M. Synergistic Antibacterial Activity of Biogenic AgNPs with Antibiotics against Multidrug Resistant Bacterial Strains. *Journal of King Saud University - Science* **2024**, *36* (10), No. 103461.
(48) Vijayaraghavan, K.; Ashokkumar, T. Plant-Mediated Biosynthesis of Metallic Nanoparticles: A Review of Literature, Factors Affecting Synthesis, Characterization Techniques and Applications. *Journal of Environmental Chemical Engineering* **2017**, *5* (5), 4866−4883.
(49) Worakitjaroenphon, S.; Shanmugam, P.; Boonyuen, S.; Smith, S. M.; Chookamnerd, K. Green Synthesis of Silver and Gold Nanoparticles Using Oroxylum Indicum Plant Extract for Catalytic and Antimicrobial Activity. *Biomass Conv. Bioref.* **2023**.
(50) Saed, M.; Ayivi, R. D.; Wei, J.; Obare, S. O. Gold Nanoparticles Antibacterial Activity: Does the Surface Matter? *Colloid and Interface Science Communications* **2024**, *62*, No. 100804.
(51) Thangamani, N.; Bhuvaneshwari, N. Green Synthesis of Gold Nanoparticles Using *Simarouba Glauca* Leaf Extract and Their Biological Activity of Micro-Organism. *Chem. Phys. Lett.* **2019**, *732*, 136587.
(52) Emmanuel, R.; Saravanan, M.; Ovais, M.; Padmavathy, S.; Shinwari, Z. K.; Prakash, P. Antimicrobial Efficacy of Drug Blended Biosynthesized Colloidal Gold Nanoparticles from *Justicia Glauca* against Oral Pathogens: A Nanoantibiotic Approach. *Microbial Pathogenesis* **2017**, *113*, 295−302.
(53) Shanmugam, P.; Murthy, A. P.; Theerthagiri, J.; Wei, W.; Madhavan, J.; Kim, H.-S.; Maiyalagan, T.; Xie, J. Robust Bifunctional Catalytic Activities of N-Doped Carbon Aerogel-Nickel Composites for Electrocatalytic Hydrogen Evolution and Hydrogenation of Nitrocompounds. *Int. J. Hydrogen Energy* **2019**, *44* (26), 13334−13344.
(54) Parameswaran, S.; Bakkiyaraj, R.; Shanmugam, P.; Boonyuen, S.; Venugopal, T. Investigation of Biological Efficacy Assessment of Cobalt-Doped Cerium Oxide Nanocomposites against Pathogenic Bacteria, Fungi, and Lung Cancer Cells. *Mater. Chem. Phys.* **2024**, *321*, No. 129496.

https://doi.org/10.1021/acsomega.4c10323
ACS Omega 2025, 10, 17327−17336